RSC Advances

PAPER

View Article Online
View Journal | View Issue

Cite this: *RSC Adv.*, 2017, **7**, 7179

Novel three-dimensional island-chain structured V_2O_5/graphene/MWCNT hybrid aerogels for supercapacitors with ultralong cycle life

Wenchao Bi, Guohua Gao,* Yingjie Wu, Huiyu Yang, Jichao Wang, Yuerou Zhang, Xing Liang, Yindan Liu and Guangming Wu*

Received 11th October 2016
Accepted 7th November 2016

DOI: 10.1039/c6ra25077g

www.rsc.org/advances

Novel three-dimensional (3D) island-chain structured vanadium pentoxide (V_2O_5)/graphene (GN)/multiwalled carbon nanotube (MWCNT) hybrid aerogels (VGMA) are synthesized by a sol–gel method. In this process, V_2O_5 *in situ* grows along the surface of both MWCNT and GN by the coordination effect. These two kinds of one-dimensional fibers (V_2O_5 nanofibers and V_2O_5 coated MWCNT) and one kind of two-dimensional sheets (GN) co-assemble into a 3D porous island-chain structure. VGMA exhibit enhanced specific capacitance (504 F g^{-1}), large energy density (70 W h kg^{-1}) and outstanding cyclic property (82.9% retention after 32 500 cycles). All these excellent electrochemical properties of ternary VGMA can be attributed to the well-designed nanostructure and synergistic effect of the individual components. This also demonstrates that the unique island-chain nanostructured VGMA can be a good candidate for supercapacitors.

1 Introduction

With the growing energy crisis, there is an urgent demand for environmentally friendly, high-performance energy storage for various portable electronic devices, hybrid motor vehicles, large industrial equipment and military devices.[1,2] Lithium batteries and supercapacitors are two major devices for electric energy storage. Supercapacitors, as a new type of energy storage device, have drawn more attention than lithium batteries for high power density, long cyclic life, rapid charging–discharging rate and low cost. According to the charge storage mechanism, supercapacitors are categorized into two types: one is electrical double layer capacitors (EDLCs) which result from the accumulation of electrons at the electrode–electrolyte interface. The other type is pseudocapacitors where the energy storage process is based on the redox reaction of the electrode materials with the electrolyte.[3] The two types of reactions all happen near or in the electrode materials. So electrode materials can affect the electrochemical performance of supercapacitors. And the electrochemical performance can be greatly improved if the electrode materials possess high specific surface area, electrical conductivity and firm frameworks.[4–7] The electrode materials usually include carbon-based materials (*e.g.*, active carbon, graphene, multiwalled carbon nanotube, porous carbon), transition metal oxides (*e.g.*, MnO_2, RuO_2, Co_3O_4) and conducting polymers (*e.g.*, polypyrrole, polyaniline).

Vanadium pentoxide (V_2O_5), a kind of transition metal oxide, is one of the promising candidates with the advantages of high theoretical specific capacitance (2120 F g^{-1}), multiple oxidation states, low cost and abundant resources.[8] However, low electrical conductivity, limited specific surface area and less efficient pseudocapacitive contribution restrict its application in high-performance supercapacitors.[3] To overcame these weaknesses, lots of other binary V_2O_5 materials have also been designed and composited with carbonaceous materials, such as intertwined V_2O_5 nanowires/MWCNTs,[9] V_2O_5 nanowires/GN composites,[10] rod-like V_2O_5/GN composites,[11] V_2O_5/porous carbons composites.[12] Though these binary composites on V_2O_5 and carbon improved the electrical conductivity and electrochemical performance, the specific capacitance and cycling life still cannot meet daily requirements. Moreover, Gleb Yushin *et al.*[13] prepared binary V_2O_5/MWCNTs by atomic layer deposition to improve electrical conductivity and cycle stability. Although the composite achieved a high specific capacitance, the efficient pseudocapacitive contribution of vanadium was reduced greatly. Compared with binary composites, ternary composites possess many advantages when applied in supercapacitors, such as 3D structure, hierarchical porosity and high contacting efficiency.[14] And ternary metal oxide composites with unique structures can offer more references for better electrochemical performances for storage devices. For instance, Chao *et al.*[15] prepared ternary core–shell structured graphene/V_2O_5/conductive-polymer *via* template method as high-performance electrode material of lithium batteries. But the whole synthesis progress is complicated, time-consuming and cannot be prepared at ambient environment. And Mai *et al.*[16] designed

Shanghai Key Laboratory of Special Artificial Microstructure, School of Physics Science and Engineering, Tongji University, Shanghai, 200092, PR China. E-mail: gao@tongji.edu.cn; gmwu@tongji.edu.cn

cucumber-like V_2O_5/PEDOT/MnO_2 for lithium batteries. The stable framework, high active surface area and short ion diffusion path caused by the novel structure also enhance electrochemical performance and cycling life. Pan Xiong *et al.*[17] designed sandwich nanostructured manganese ferrite/GN/polyaniline composites for supercapacitors. And superiority of each component was fully utilized, showing higher specific capacitance (454.8 F g^{-1}) and better cycling stability (76.4% retention after 5000 cycles) than graphene/polyaniline hybrids. All these ternary metal oxide composites with novel nanostructures were proven to effective to improve electrochemical performance. In addition, ternary conducting polymer/GN/MWCNT composites were also obtained with enhanced electrochemical performances, like GS/PPy/CNT composites,[18] PANI/GS/CNT.[19] Considering the extraordinary conductivity and mechanical properties of MWCNT[20] and GN,[21] ternary V_2O_5, GN and MWCNT hybrid aerogels with intriguing structure may achieve enhanced electrochemical performance compared with individual components. Since it is hard to achieve well dispersity and design an ideal structure, few studies on the ternary V_2O_5, GN and MWCNT composite have been reported so far. Therefore, preparing ternary V_2O_5, GN and MWCNT composite is a desirable work.

In this text, the novel island-chain structured V_2O_5/GN/MWCNT aerogels (VGMA) were synthesized, for the first time to the best of our knowledge, *via* a one-step sol–gel method. The unique 3D island-chain structure is successfully and uniformly co-assembled by three kinds of different dimensional materials: V_2O_5 nanofibers (1D), carbon nanotubes (1D) and graphene sheets (2D). And tested for supercapacitors, VGMA hybrid aerogels exhibit enhanced electrochemical performance and ultralong cycle life due to the novel nanostructure.

2 Experimental

2.1 Synthesis of V_2O_5 sol

Commercial V_2O_5 powder was used to prepare the functional V_2O_5 sol. First, raw V_2O_5 powder, benzyl alcohol and isopropanol were mixed at a molar ratio of 1 : 4 : 40. Then the mixture was kept at 90 °C with a condenser for 4 h. Unreacted V_2O_5 was filtered out for recycling and the remaining pale yellow sol was concentrated to 1/3 volume through heating reflux. Eventually, a faint yellow functional V_2O_5 sol composed of vanadium oxide (VO_x) oligomers was obtained and the content of V_2O_5 was about 30 mg ml^{-1}.[22]

2.2 Fabrication of VGMA island-chain hybrid aerogels

Graphene oxide (GO) was prepared from natural graphite flakes by a modified Hummers method.[23] Functional MWCNT was obtained after mixed acid (H_2SO_4 : HNO_3 = 3 : 1) treatment.[24] GO and MWCNT were added into deionized water at a mass ratio of 1 : 1 and ultrasonically treated to form a homogeneous dispersion. Then, 15 ml GO/MWCNT hybrid aqueous dispersion was added into 10 ml as-prepared V_2O_5 sol under vigorous stirring. About 20 min later, VO_x/GO/MWCNT gel was obtained and aged for 2 days at 50 °C. After solvent replacement and freeze drying processes, the gel was heated in air at 300 °C for 3 hours. Finally, crystalline VGMA hybrid aerogels were successfully synthesized. And V_2O_5 aerogels were also obtained under the same condition without GN and MWCNT as a contrast.

2.3 Characterizations

Raman spectra (Jobin-Yvon HR800) were recorded from 100 to 2000 cm^{-1} using a 514 nm argon ion laser. X-ray powder diffraction (XRD) patterns were obtained by using a Rigaku D/max-C diffractometer with a Cu Kα radiation source (λ = 1.5406 Å). Nitrogen adsorption isotherms were measured using an Autosorb-1 (Quanta-chorme) analyzer. The morphologies and structures of the samples were systematically investigated by field emission scanning electron microscopy (FESEM, S-4800), transmission electron microscopy (TEM, JEOL-2100) and high-resolution transmission electron microscopy (HRTEM, field emission JEOL-2100).

2.4 Electrochemical measurements

A symmetrical two-electrode configuration in 1 M Na_2SO_4 aqueous electrolyte was chosen to confirm VGMA a good candidate as electrode material for supercapacitors.[22,25] The electrodes were prepared by homogeneous mixing active materials, acetylene black and poly(vinylidene fluoride) (PVDF) dispersed in *N*-methylpyrrolidone (NMP) at the mass ratio of 8 : 1 : 1. The obtained mixture was coated onto graphite papers (1 cm × 3 cm) and the area is about 1 cm^2, and finally dried in a vacuum oven at 120 °C for 12 hours. The potentials of the VGMA supercapacitor electrode materials were evaluated by cyclic voltammetry (CV) and galvanostatic charge/discharge with a CHI 660C electrochemical workstation. The working potential was set from −1 to 1 V.[25,26] To obtain the specific capacitance for a single electrode (C, F g^{-1}) from the galvanostatic discharge curves, we used the formula $C = 2/\Delta t/\Delta V$. The energy density and powder density in Ragone plots were respectively calculated by the formula $E = (1/8)C(\Delta V)^2/3600$ and $P = E/\Delta t$, where I referred to the constant discharging current density based on the total mass of a single electrode, Δt was the discharging time and ΔV was the potential window, respectively.[27,28] Electrochemical impedance spectroscopy (EIS) measurements were performed by a CHI 660C electrochemical workstation with the frequency ranging from 0.01 Hz to 100 kHz and the AC amplitude 5 mV. To research whether the electrochemical performances were enhanced, raw V_2O_5 powder and pure V_2O_5 aerogels were also tested under the same condition for supercapacitors.

3 Results and discussion

In the traditional sol–gel progress, the hydrolysis and condensation happened in rather short time. As the vanadium oxide (VO_x) oligomers hydrolyzed, vanadium appeared as a six-fold coordination with one water molecule along the z axis and a short V=O double bond in the opposite direction. In the equatorial plane, another water molecule was in the x axis, one –OH group in opposite direction and two –OH groups in the y

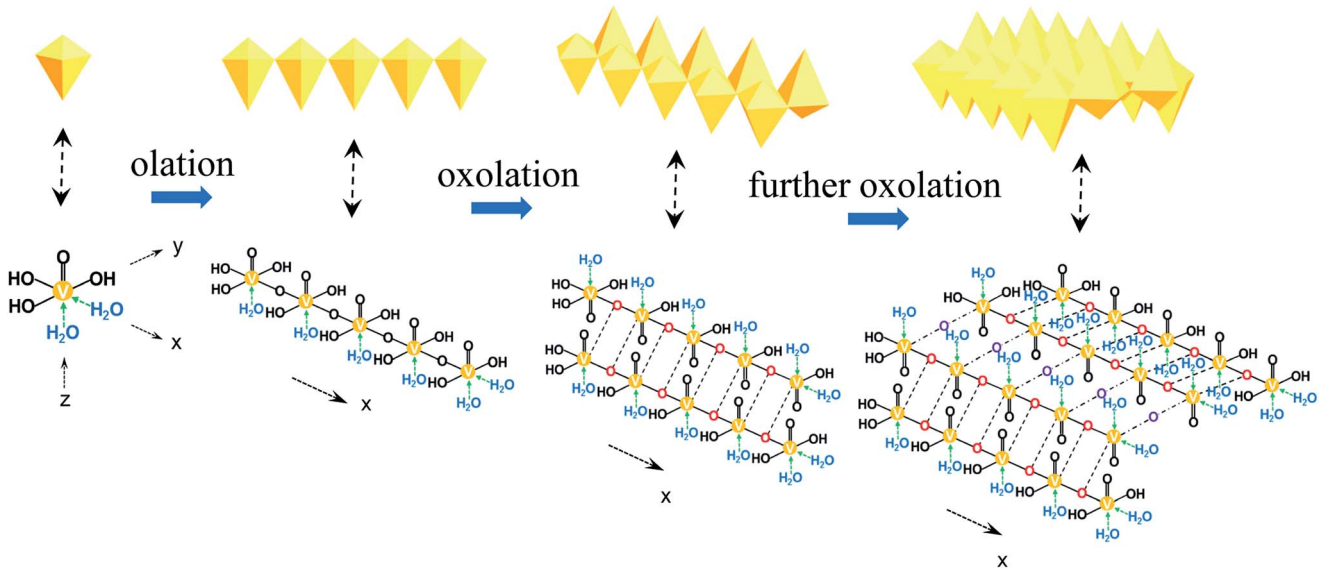

Fig. 1 The formation of V_2O_5 nanofiber.

axis (Fig. 1a). Since the length of V–O bond was not equal in the *x* and *y* directions, condensation occurred more rapidly in the *x* direction between H_2O–V-OHs, forming the olation chain polymers (Fig. 1b). And slower condensation took place in HO–V-OHs by oxolation in the *y* axis, resulting in double chain polymers as shown in Fig. 1c. At last, these double chains were linked together by further condensations between the other –OH groups (Fig. 1d).[8,29] When aging was extended, V_2O_5 nanofibers formed due to the preferred growth.

We synthesized the 3D porous island-chain hybrid aerogels by pouring the GO and MWCNT hybrid aqueous dispersion into the as-prepared V_2O_5 sol. The carboxyl (–COOH) and hydroxyl (–OH) groups on GO surfaces make GO highly negatively charged when dispersed in water, the same with acid-treated MWCNTs modified with –OH or –COOH on the surface.[30–32] So the electrostatic repulsion enables the formation of GO and MWCNT hybrid aqueous dispersion without aggregation. When the aqueous dispersion was added into the V_2O_5 sol, the VO_x oligomers began to hydrolyze and the unique 3D island-chain structure of VGMA formed through the following different formation progresses by coordination bonds (shown in Fig. 2): (i) pure V_2O_5 fibers: as in the conventional hydrolysis procedure of V_2O_5 sol mentioned above, VO_x oligomers coordinated with –OH in H_2O molecules and the pure V_2O_5 nanofibers were built by condensation reactions through olation and oxolation. (ii) Core–shell structured MWCNTs coated by V_2O_5: coordination also happened among some VO_x oligomers and –OH, –COOH groups introduced by acid-treated MWCNTs. So VO_x oligomers condensed and *in situ* grew along MWCNTs *via* olation and oxolation, forming the core–shell structure with V_2O_5 as shell. (iii) V_2O_5 nanofibers anchored on surfaces of GO sheets. The other VO_x oligomers were anchored on the GO surface by coordination bonds (–OH, –COOH) of GO during the *in situ* rapid condensation reactions. All the condensation reactions described above occurred simultaneously in the sol–gel process. (iv) 3D island-chain architecture by co-assembling: as the aging extending, MWCNTs from (ii) were completely coated by V_2O_5. And at the same time, the length and diameter of V_2O_5 nanofibers from both (i) and (iii) further increased. These V_2O_5 nanofibers and MWCNTs interconnected with each other and also linked these separated island-like GO sheets together, co-assembling the island-chain architecture. Thus, two kinds of 1D nanofibers (V_2O_5, MWCNTs) and 2D nanosheets (GN) co-assembled into a unique 3D porous island-chain framework.

To investigate the structural incorporation of the VGMA aerogels, Raman test results are shown in Fig. 3a. Peaks at 140, 281, 407, 529, 693 and 996 cm^{-1} of the VGMA hybrid aerogels correspond to the skeleton bending vibrations of the V–O–V bonds, bending vibrations of V=O bonds, bending vibrations of bridge oxygen bonds, stretching vibrations of chain oxygen bonds, stretching vibrations of doubly coordinated oxygen and in-phase stretching vibrations of V=O bonds, respectively. The characteristic peaks at 1349 and 1579 cm^{-1} detected in the VMGA hybrid aerogels are D and G bands of GN and MWCNT, respectively,[33,34] confirming the existence of GN and MWCNT. All these validate the perfect structural integrity of the V_2O_5, GN and MWCNT.

XRD measurements were used to obtain the crystal phase and structure information of the samples. Fig. 3b shows XRD patterns of V_2O_5, V_2O_5 aerogel, GO and VGMA. The main peaks of VGMA agree with that of V_2O_5 and V_2O_5 aerogel.[35,36] Besides the easily recognized diffraction peaks of V_2O_5, no conventional stacking peaks of GO or MWCNT were detected in the VGMA composite, suggesting that GO has been reduced and the residual GN sheets may be individual monolayers that homogeneously dispersed in the resulting 3D framework.[37,38]

The BJH pore size distribution (in Fig. 3c) and nitrogen isotherm (Fig. 3d) indicate VGMA possess porous structure by the presence of micropores, mesopores and macropores.[36,39] It is attributed to the island-chain framework of VGMA built by

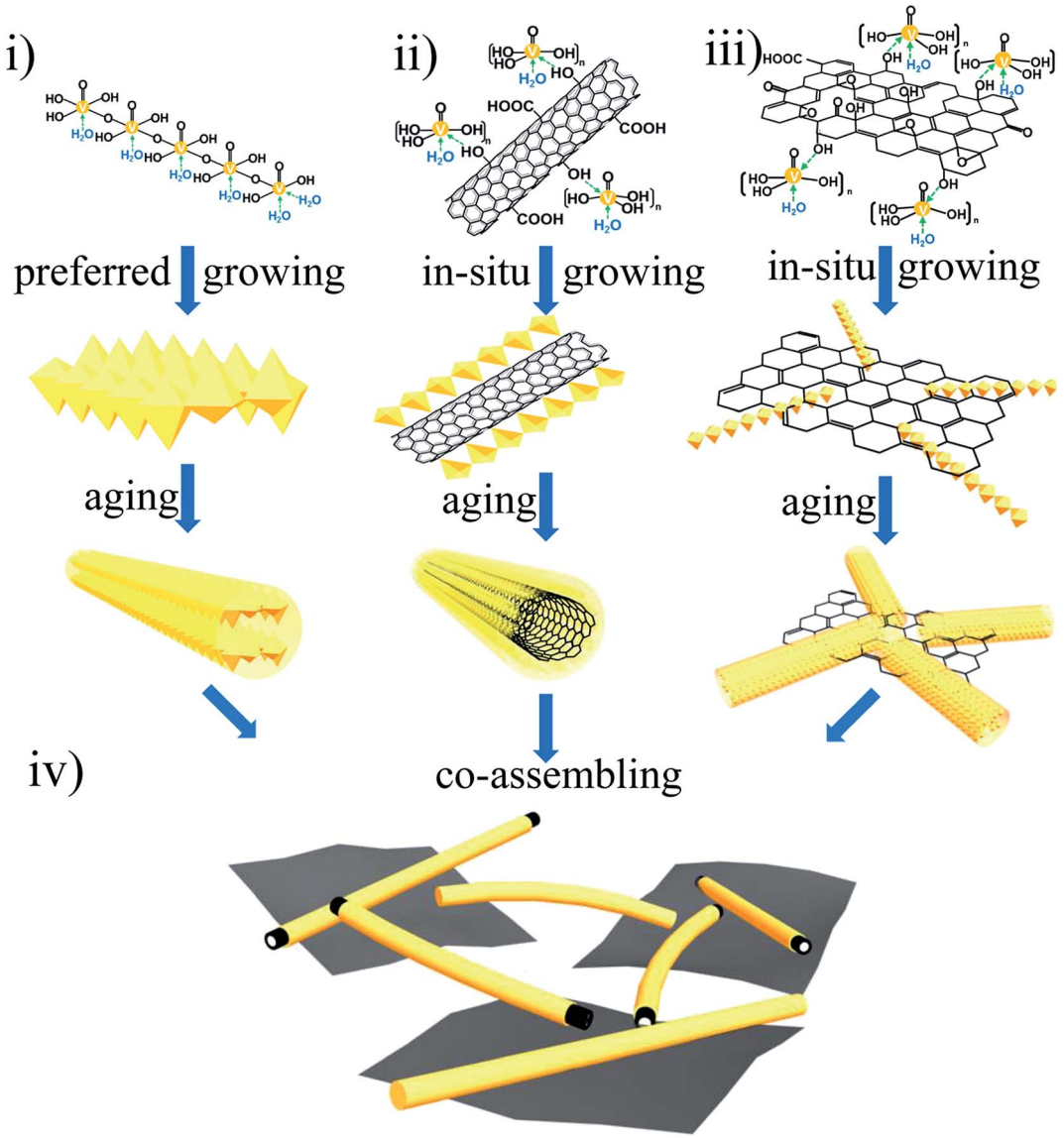

Fig. 2 The schematic of the island-chain structured VGMA.

the co-assembling of V_2O_5 fibers, GN sheets and MWCNTs. That is to say, both the anchoring of V_2O_5 fibers on the GN and interconnection of MWCNTs and V_2O_5 creates abundant pores and space. The porous structure also increases the specific surface area of VGMA to 310 $m^2\ g^{-1}$, much higher than that of V_2O_5 aerogels (35 $m^2\ g^{-1}$), V_2O_5/GN aerogels (172 $m^2\ g^{-1}$)[22] and V_2O_5/MWCNT aerogels (61 $m^2\ g^{-1}$).[40] The high specific surface area can enlarge interface of electrode material–electrolyte to facilitate the redox reaction and the accumulation of electrons, enhancing the capacitive performances. It worth noting that, the VGMA show low density at 24.3 mg cm^{-3} due to the unique 3D porous structure. The density of VGMA is larger than that of V_2O_5 aerogels (23.4 mg cm^{-3}) synthesized under the same condition because of the addition of GO and MWCNTs. But the pure V_2O_5 aerogel bulk (inserted in Fig. 4a) is extremely fragile and unstable. It is a challenge to prepare uncracked, robust and stable metal aerogels with density below 25 mg cm^{-3}.[40,41] VGMA are also lighter than V_2O_5/GN aerogels (27.7 mg cm^{-3}),[22] V_2O_5/MWCNT aerogels (27.3 mg cm^{-3})[40] and other metal aerogels, such as Al_2O_3 aerogel (93 mg cm^{-3}), CuO aerogel (267 mg cm^{-3}), TiO_2 aerogel (145 mg cm^{-3}), ZrO_2 aerogel (446 mg cm^{-3}) and Cr aerogel (230 mg cm^{-3}).[41–45] Fig. 4a shows that VGMA are light enough that can be held on a feather. Moreover, with the addition of GN and MWCNT, VGMA overcome the difficulty and exhibit uncracked, robust and stable, which are proven by supporting 100 g weight (Fig. 4b).

The morphology and structure of VGMA were investigated. Compared with pure V_2O_5 aerogels by SEM (Fig. 5b), the VGMA hybrid aerogels show a unique 3D structure in SEM (Fig. 5a), TEM (Fig. 4c) and HRTEM (Fig. 4d) patterns: V_2O_5 nanofibers and MWCNTs interconnect with each other, and some V_2O_5 nanofibers *in situ* grow along the GN nanosheets. These separated island-like GN nanosheets are jointed together by the chain-like V_2O_5 nanofibers and MWCNTs. The HRTEM image is

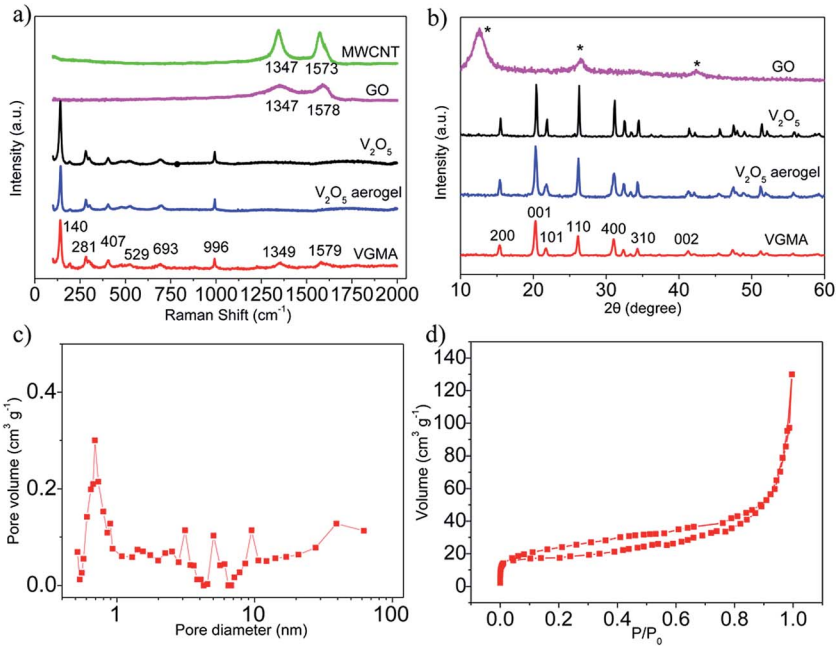

Fig. 3 (a) Raman spectra of V_2O_5, V_2O_5 aerogel, MWCNT, GO and VGMA (b) XRD patterns of V_2O_5, V_2O_5 aerogel, GO and VGMA (c) BJH pore-size distribution plot of VGMA (d) nitrogen absorption–desorption isotherm of VGMA.

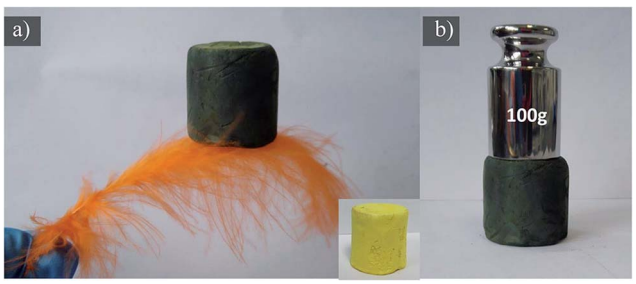

Fig. 4 (a) The VGMA which are so light that can be lifted by a feather and the V_2O_5 aerogels are inserted (b) the digital photo of VGMA holding 100 g weight.

used to further exhibit the microstructure of VGMA. It can be clearly observed that the MWCNT is coated by V_2O_5 uniformly and the coating thickness of V_2O_5 is about 2–3 nm. All these images confirm the 3D porous island-chain structures we supposed above.

To verify the VGMA promising candidate for supercapacitors, electrochemical measurements were carried out. Fig. 6a exhibits the CV curves of V_2O_5, V_2O_5 aerogel and VGMA at scan rate 5 mV s^{-1}. Obviously, the CV curve of VGMA appears as near a rectangular shape, showing capacitance characteristics. Redox peaks and the near rectangular shapes show the synergy of the pseudocapacitors (V_2O_5) and double layer capacitors (GN and MWCNT).[13,22,40] Since the specific capacitance is proportional to the area of CV curve, the largest curve area also indicates that WMNA possess larger specific capacitance than that of raw V_2O_5 powder and V_2O_5 aerogels. This may be a consequence of developed surface area, the synergistic effect and improved the electrical conductivity by GN and MWCNT. The CV curves of V_2O_5, V_2O_5 aerogel and VGMA under various sweep rates are respectively shown in Fig. 6b–d. The similar shapes of VGMA in CV images at different sweep rates suggest a nice specific capacitance property and the fast diffusion of electrolyte ions.

To obtain specific capacitances, galvanostatic charge/discharge curves of V_2O_5, V_2O_5 aerogel and VGMA at a current density of 0.5 A g^{-1} are tested (Fig. 7a). The charge/discharge curves at different current densities (Fig. 7b–d) are not perfectly linear, showing the typical pseudocapacitive behavior with a slope variation of time dependence of the potential. The calculated specific capacitance of VGMA is 504 F g^{-1}, which is much higher than raw V_2O_5 (169 F g^{-1}) and V_2O_5 aerogels (251 F g^{-1}) at a current density of 0.5 A g^{-1}. These results are in accordance with those deduced from CV curves. Compared with V_2O_5/GN aerogels (486 F g^{-1}),[22] VGMA show higher specific capacitance than V_2O_5/GN aerogels because excess V_2O_5-coated MWCNTs act as "chain" between separated GN sheets and improve the conductivity by providing better conductive pathways for the transport of electron. The specific capacitance of VGMA is still higher than V_2O_5/MWCNT aerogels with the equivalent content of MWCNT (410 F g^{-1}). Though V_2O_5/MWCNT aerogels can reach higher specific capacitance with more MWCNTs, the excess content of MWCNT may reduce the specific surface area, enlarge the density and weaken the capacitive performance of VGMA.[40,46]

Fig. 8a shows the specific capacitances of V_2O_5, V_2O_5 aerogels and VGMA at different current densities. Obviously, the specific capacitances of VGMA at different current densities are all clearly larger than V_2O_5 powder and V_2O_5 aerogels, suggesting a high-rate performance under high current density. In the Ragone plots of the supercapacitors based on V_2O_5, V_2O_5

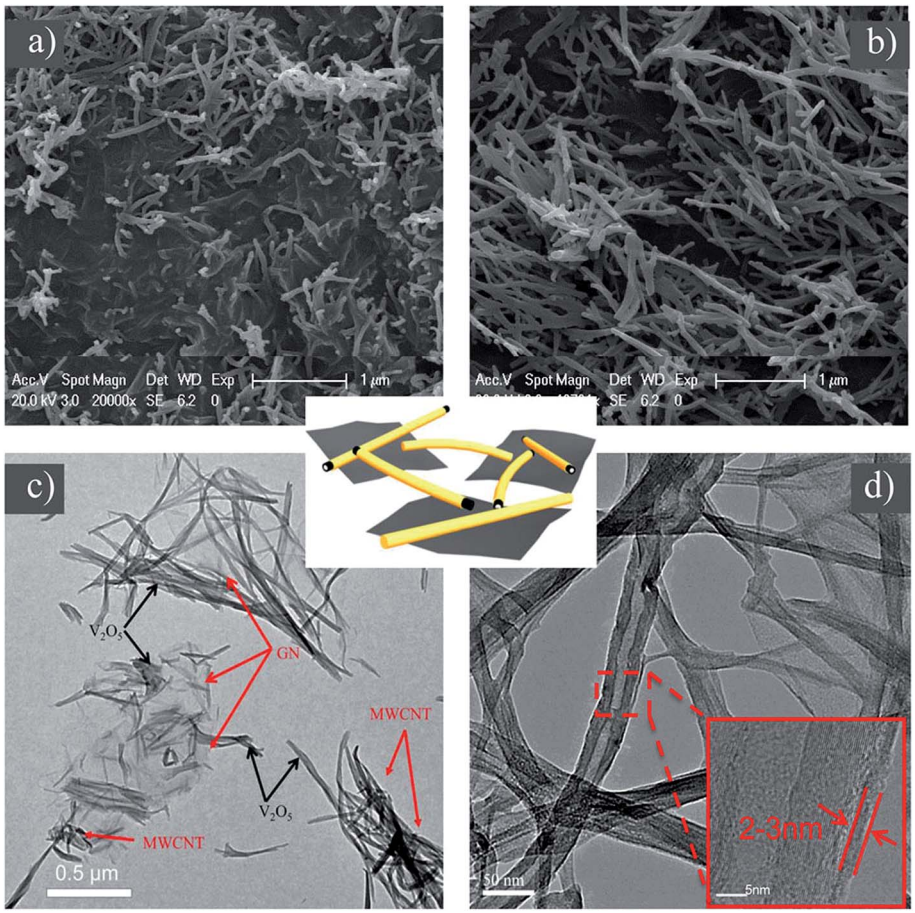

Fig. 5 (a) SEM of VGMA (b) SEM of V_2O_5 aerogel (c) TEM of VGMA (d) HRTEM of VGMA. The schematic of island-chain structure is in the middle.

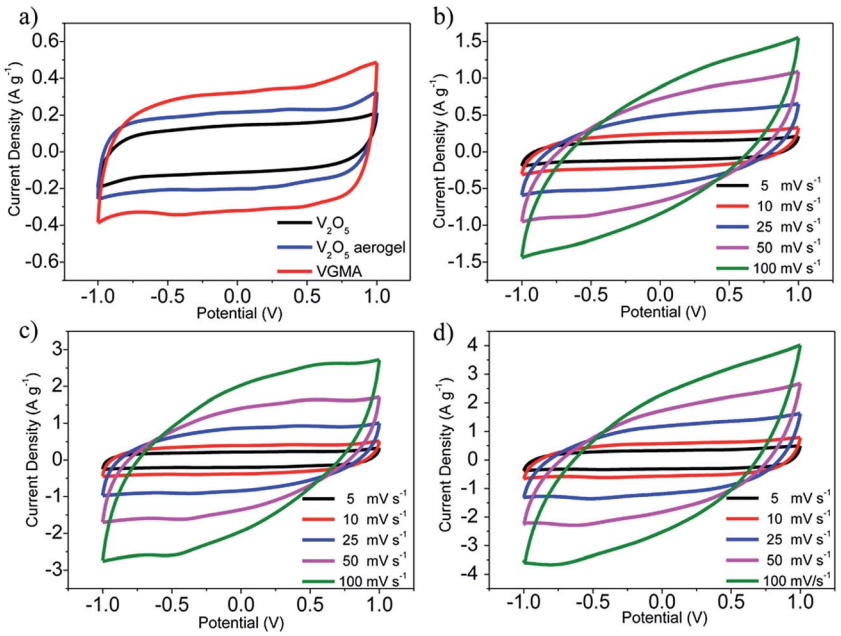

Fig. 6 (a) CV curves of V_2O_5 powder, V_2O_5 aerogel and VGMA at 5 mV s^{-1} (b–d) CV curves of V_2O_5 powder, V_2O_5 aerogel and VGMA at different sweep rates.

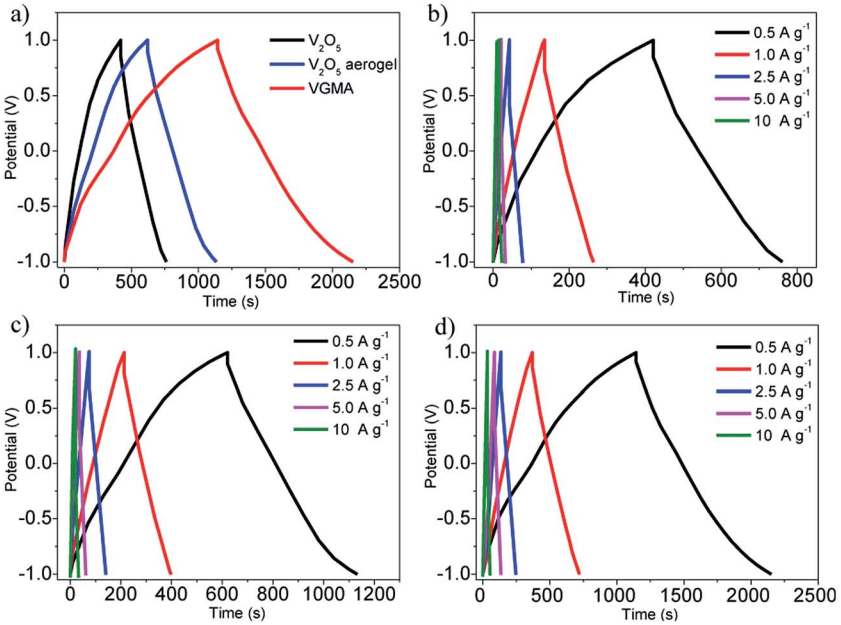

Fig. 7 (a) Galvanostatic charge/discharge curve of VGMA at a current density of 0.5 A g^{-1} (b–d) galvanostatic charge/discharge curves of V_2O_5, V_2O_5 aerogel and VGMA at different current densities, respectively.

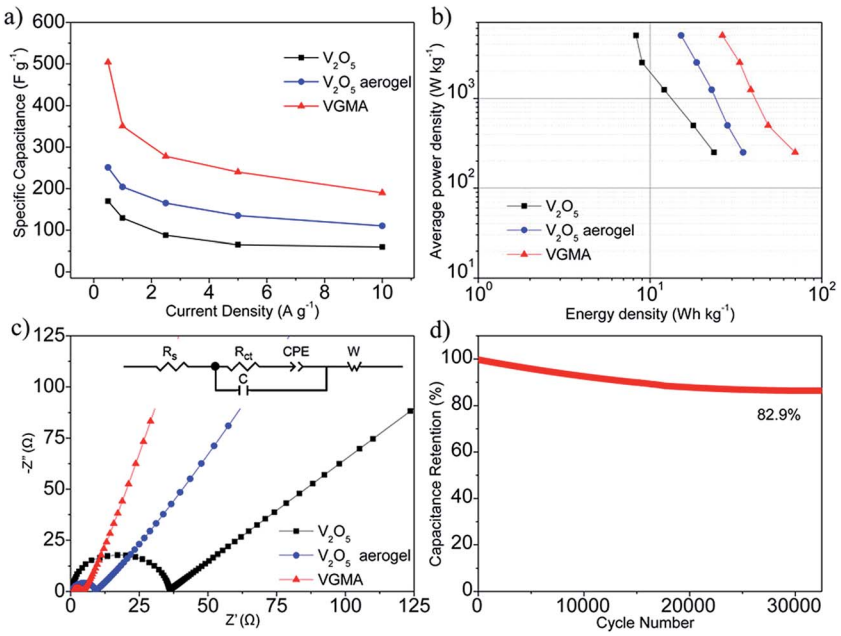

Fig. 8 (a) The specific capacitances of V_2O_5, V_2O_5 aerogel and VGMA at different current densities (b) Ragone plots of the supercapacitors based on V_2O_5, V_2O_5 aerogel and VGMA (c) EIS spectra of V_2O_5, V_2O_5 aerogel and VGMA (d) the cycling performance of VGMA after 32 500 circulations.

aerogel and VGMA (Fig. 8b), VGMA possess larger energy density of 70 W h kg^{-1} with average powder density 250 W kg^{-1}. EIS spectra of V_2O_5, V_2O_5 aerogel and VGMA (Fig. 8c) prove that the addition of GN and MWCNT reduces the charge transfer resistance of VGMA to 4.3 Ω, while V_2O_5 powder is 38.6 Ω and V_2O_5 aerogel is 9.1 Ω. The improved electrical conductivity is mainly due to excellent electronical conductivity of the GN and MWCNT and the island-chain conductive structure. That is to say, chain-like MWCNT, island-like GN and the core/shell V_2O_5/MWCNT corporately shorten the charge transfer distance and offer pathways for electron transfer. To explore more electrochemical properties of VGMA, cycling property was tested at a large current density of 10 A g^{-1}. As shown in Fig. 8d, the specific capacitance remains about 82.9% of initial value after 32 500 charge/discharge circulations, which is attributed to the unique porous structure of the hybrid aerogels.[13] The unique

structure can increase the electrolyte–electrode interfacial area, make the charge transfer distance shorter and facilitate the electrolyte wetting. Moreover, the addition of GN and MWCNT can improve the electronical conductivity. Thus, the electrochemical performance can be enhanced even at a large current density (10 A g^{-1}). In addition, it is noteworthy that the cycling property of island-chain structured VGMA is superior to that of other reported vanadium-based electrode materials, such as V_2O_5 anchored MWCNTs (60% remained after 25 cycles),[47] V_2O_5 nanowires/MWCNTs (50% remained after 5000 cycles),[9] core–shell structured V_2O_5/MWCNTs (92% remained after 5000 cycles),[13] V_2O_5 nanowires/GN (60% remained after 50 cycles),[10] rod-like V_2O_5/GN composites (82.9% remained after 1000 cycles),[11] V_2O_5/GN aerogels (90% remained after 20 000 cycles).[22] Therefore, the novel ternary porous island-chain structured vanadium-based electrode material can be a potential candidate for high-performance supercapacitors. And it is significant for more creative synthesis of supercapacitor electrode materials.

4 Conclusions

In summary, the novel 3D porous island-chain VGMA hybrid aerogels were synthesized *via* a low-cost and facilitated sol–gel method for the first time. We designed novel structure *via in situ* growth of V_2O_5 on the surface of graphene and MWCNTs simultaneously and eventually they co-assembled into the island-chain structure. And electrochemical measurements on the VGMA electrodes showed enhanced specific capacitance (504 F g^{-1} with the current density of 0.5 A g^{-1}), high energy density (70 W h kg^{-1}) and extremely excellent cycle stable performance (82.9% of initial specific capacitance after 32 500 cycles) due to the unique structure and synergistic effect. The ternary island-chain VGMA validated the nanocomposite approach for electrode materials of high-performance supercapacitors. And we believe that VGMA can be used in many applications due to the novel structure, like lithium batteries, absorbents, sensors and analysis.

Acknowledgements

The authors sent grateful acknowledgements for the financial support from Fundamental Research Funds for the Central Universities, and the National Natural Science Foundation of China (51472182, 51272179 and U1503292).

References

1 S. Chu and A. Majumdar, *Nature*, 2012, **488**, 294–303.
2 S. Yang, Y. Gong, Z. Liu, L. Zhan, D. P. Hashim, L. Ma, R. Vajtai and P. M. Ajayan, *Nano Lett.*, 2013, **13**, 1596–1601.
3 M. J. Zhi, C. C. Xiang, J. T. Li, M. Li and N. Q. Wu, *Nanoscale*, 2013, **5**, 72–88.
4 R. Kotz and M. Carlen, *Electrochim. Acta*, 2000, **45**, 2483–2498.
5 G. P. Wang, L. Zhang and J. J. Zhang, *Chem. Soc. Rev.*, 2012, **41**, 797–828.
6 P. Simon and Y. Gogotsi, *Nat. Mater.*, 2008, **7**, 845–854.
7 Y. He, W. Chen, C. Gao, J. Zhou, X. Li and E. Xie, *Nanoscale*, 2013, **5**, 8799–8820.
8 V. Augustyn and B. Dunn, *C. R. Chim.*, 2010, **13**, 130–141.
9 Z. Chen, V. Augustyn, J. Wen, Y. Zhang, M. Shen, B. Dunn and Y. Lu, *Adv. Mater.*, 2011, **23**, 791–795.
10 S. D. Perera, M. Rudolph, R. G. Mariano, N. Nijem, J. P. Ferraris, Y. J. Chabal and K. J. Balkus, *Nano Energy*, 2013, **2**, 966–975.
11 M. Li, G. Sun, P. Yin, C. Ruan and K. Ai, *ACS Appl. Mater. Interfaces*, 2013, **5**, 11462–11470.
12 H. Yamada, F. Nakahara, I. Moriguchi and T. Kudo, *J. Phys. Chem. C*, 2007, **111**, 227–233.
13 S. Boukhalfa, K. Evanoff and G. Yushin, *Energy Environ. Sci.*, 2012, **5**, 6872–6879.
14 A.-H. Lu, G.-P. Hao, Q. Sun, X.-Q. Zhang and W.-C. Li, *Macromol. Chem. Phys.*, 2012, **213**, 1107–1131.
15 D. Chao, X. Xia, J. Liu, Z. Fan, C. F. Ng, J. Lin, H. Zhang, Z. X. Shen and H. J. Fan, *Adv. Mater.*, 2014, **26**, 5794–5800.
16 L. Q. Mai, F. Dong, X. Xu, Y. Luo, Q. An, Y. Zhao, J. Pan and J. Yang, *Nano Letters*, 2013, **13**, 740–745.
17 P. Xiong, C. Hu, Y. Fan, W. Zhang, J. Zhu and X. Wang, *J. Power Sources*, 2014, **266**, 384–392.
18 B. Wang, J. Qiu, H. Feng and E. Sakai, *Electrochim. Acta*, 2015, **151**, 230–239.
19 S. Zhou, H. Zhang, X. Wang, J. Li and F. Wang, *RSC Adv.*, 2013, **3**, 1797–1807.
20 Q. Lu, J. G. Chen and J. Q. Xiao, *Angew. Chem., Int. Ed.*, 2013, **52**, 1882–1889.
21 V. C. T. Matthew, J. Allen and R. B. Kaner, *Chem. Rev.*, 2010, **110**, 132–145.
22 Y. J. Wu, G. H. Gao and G. M. Wu, *J. Mater. Chem. A*, 2015, **3**, 1828–1832.
23 W. S. Hummers and R. E. Offeman, *J. Am. Chem. Soc.*, 1958, **6**, 1339–1340.
24 V. Datsyuk, M. Kalyva, K. Papagelis, J. Parthenios, D. Tasis, A. Siokou, I. Kallitsis and C. Galiotis, *Carbon*, 2008, **46**, 833–840.
25 Y. J. Wu, G. H. Gao, H. Y. Yang, W. Bi, X. Liang, Y. Zhang, G. Zhang and G. Wu, *J. Mater. Chem. A*, 2015, **3**, 15692–15699.
26 J. X. Zhu, L. J. Cao, Y. S. Wu, Y. J. Gong, Z. Liu, H. E. Hoster, Y. H. Zhang, S. T. Zhang, S. B. Yang, Q. Y. Yan, P. M. Ajayan and R. Vajtai, *Nano Lett.*, 2013, **13**, 5408–5413.
27 X. B. Wang, Y. J. Zhang, C. Y. Zhi, X. Wang, D. Tang, Y. Xu, Q. Weng, X. Jiang, M. Mitome, D. Golberg and Y. Bando, *Nat. Commun.*, 2013, **4**, 2905.
28 X. W. Yang, Y. Wang, L. Qiu and D. Li, *Science*, 2013, **341**, 534–537.
29 M. D. Stoller, S. J. Park, Y. W. Zhu and J. H. An, *Nano Letters*, 2008, **8**, 3498–3502.
30 O. B. Tamas Szabo and P. Forgo, *Chem. Mater.*, 2006, **18**, 2740–2749.
31 D. Li, M. B. Müller, S. Gilje, R. B. Kaner and G. G. Wallace, *Nat. Nanotechnol.*, 2008, **3**, 101–105.
32 H. H. Anton Lerf, M. Forster and J. Klinowski, *J. Phys. Chem. B*, 1998, **102**, 4477–4482.

33 J. Wang, Z. Shi, J. Fan, Y. Ge, J. Yin and G. Hu, *J. Mater. Chem.*, 2012, **22**, 22459–22466.
34 H. F. Ju, W. L. Song and L. Z. Fan, *J. Mater. Chem. A*, 2014, **2**, 10895–10903.
35 H. Liu, P. He, Z. Li, D. Sun, H. Huang, J. Li and G. Zhu, *Chem.–Asian J.*, 2006, **1**, 701–706.
36 B.-H. Kim, C. H. Kim, K. S. Yang, A. Rahy and D. J. Yang, *Electrochim. Acta*, 2012, **83**, 335–340.
37 L. L. Zhang, S. Duan, X. L. Yang, G. Peng, G. Liang, Y. H. Huang, Y. Jiang, S. B. Ni and M. Li, *ACS Appl. Mater. Interfaces*, 2013, **5**, 12304–12309.
38 H. Zhang, A. Xie, C. Wang, H. Wang, Y. Shen and X. Tian, *ChemPhysChem*, 2014, **15**, 366–373.
39 H. Wang, L. Shi, T. Yan, J. Zhang, Q. Zhong and D. Zhang, *J. Mater. Chem. A*, 2014, **2**, 4739–4750.
40 Y. J. Wu, G. H. Gao, H. Y. Yang, W. C. Bi, X. Liang, Y. R. Zhang, G. Y. Zhang and G. M. Wu, *J. Mater. Chem. A*, 2015, **3**, 15692–15699.
41 J. F. Poco, J. H. Satcher and L. W. Hrubesh, *J. Non-Cryst. Solids*, 2001, **285**, 57–63.
42 A. Du, B. Zhou, J. Shen, S. Xiao, Z. Zhang, C. Liu and M. Zhang, *J. Non-Cryst. Solids*, 2009, **355**, 175–181.
43 A. Du, B. Zhou, J. Shen, J. Gui, Y. Zhong, C. Liu, Z. Zhang and G. Wu, *New J. Chem.*, 2011, **35**, 1096–1102.
44 G. Q. Zu, J. Shen, L. P. Zou, W. Q. Wang, Y. Lian, Z. H. Zhang and A. Du, *Chem. Mater.*, 2013, **25**, 4757–4764.
45 A. Du, B. Zhou, W. Xu, Q. Yu, Y. Shen, Z. Zhang, J. Shen and G. Wu, *Langmuir*, 2013, **29**, 11208–11216.
46 Z. Chen, Y. C. Qin, D. Weng, Q. Xiao, Y. Peng, X. Wang, H. Li, F. Wei and Y. Lu, *Adv. Funct. Mater.*, 2009, **19**, 3420–3426.
47 M. Sathiya, A. S. Prakash, K. Ramesha, J. M. Tarascon and A. K. Shukla, *J. Am. Chem. Soc.*, 2011, **133**, 16291–16299.